Int. J. Heat Mass Transfer. Vol. 34, No. 2, pp. 341–356, 1991
Printed in Great Britain

0017–9310/91 $3.00+0.00

Laminar premixed flame stabilized inside a honeycomb ceramic

DAE KI MIN and HYUN DONG SHIN†
Department of Mechanical Engineering, Korea Advanced Institute of Science and Technology, P.O. Box 150, Chong Ryang, Seoul, Korea

(*Received* 4 *August* 1989 *and in final form* 7 *December* 1989)

Abstract—A laminar premixed flame inside a honeycomb ceramic is investigated experimentally and theoretically to provide the detailed data for computational approaches and to further the physical understanding of the mechanisms of heat transfer involved, particularly internal heat recirculation. The ranges of flammability and flame stability are substantially extended without any external heating. Two types of stable flame are observed; one is nearly one-dimensional in the combustor, and the other highly two-dimensional. These are also clearly distinguished by the soot lines observed in the cross-section of the combustor, and correspond to the upper and lower solutions of the theoretical analysis. Temperature measurements show a higher gas temperature than the adiabatic flame temperature, which is attributed to the internal heat recirculation. The analysis based on the one-dimensional flame theory reproduces reasonably the experimental temperature profiles and flame behaviours, and reveals that heat is recirculated to the unburned mixture both by the conduction and the radiation of the solid phase. The stable flame is also predicted in the downstream region of the combustor, but not observed in the experiment presumably due to the two-dimensional effects of heat loss. A noticeable result of this work is the existence of the flame of low burning velocity and low temperature, which is different from the excess enthalpy flame.

1. INTRODUCTION

PREMIXED combustion inside a highly porous medium is a new area of energy-related combustion technology, sharing several characteristics with those of 'excess enthalpy burning' [1, 2] and of 'radiation controlled flame' [3]. This combustion system may be a practical model to yield the fundamental physical understanding of the combustion in gas–solid two-phase systems. Unlike the ordinary premixed flame in which the heat conduction of the gas phase is only a mechanism of heat transfer to the upstream unburned mixture to sustain combustion, additional mechanisms of heat transfer are involved in this combustion system to enhance the enthalpy of the unburned mixture; heat is recirculated to the unburned mixture through the porous medium to cause the excess enthalpy burning [1], which is one of the most outstanding characteristics of this system. Recirculating heat without simultaneous dilution by the burned gases successfully extends the ranges of flammability and flame stability to burn the otherwise non-flammable mixtures of low heat content [2], which is promising in aspects of air pollution and of energy recovery from wasted gases. Another feature of this combustion system is the strong thermal radiation field established in the porous medium due to the high emissivity of the solid, which serves to recirculate heat toward the unburned mixture [3].

The potential of the excess enthalpy flame in the porous medium, since proposed by Takeno and Sato [1], has been investigated in a series of theoretical works [4, 5] to reveal that the presence of the porous medium allows the attainment of higher burning velocity and higher flame temperature than for the ordinary premixed flame. But they confined the analysis to the impractical porous medium of infinite thermal conductivity and ignored radiation heat transfer, which is a serious obstacle to the quantitative comparison with their experimental results [6]. The porous medium may be envisioned as a ceramic sponge, in which the heat transfer of the solid phase is primarily due to the radiation while the heat conduction is less dominant. Echigo [7] has demonstrated that the porous medium of an appropriate optical thickness can save a considerable amount of non-radiating gas enthalpy due to the converted radiation. A recent analytical study of Yoshizawa *et al.* [3], with rigorous treatment of radiation, elucidates the effects of the radiation heat transfer on the structure and behaviour of the premixed flame in the porous medium. The analysis in the sponge-like material, however, is imposed on the inevitable uncertainties of the physical parameters such as the effective thermal conductivity, the radiative properties and the heat transfer coefficient, which produces rather qualitative results. As pointed out by Wang and Tien [8], furthermore, the effects of scattering which are not negligible in some porous materials may complicate the mathematical formulation too much to allow it to be solved.

The practical combustors in which the flame is stabilized may be made of narrow alumina tubes [6], of

† Author to whom correspondence should be addressed.

NOMENCLATURE

A	cross-sectional area [m^2]
B	frequency factor in Arrhenius rate expression [$m^{-3} s^{-1}$]
Bo	Boltzmann number defined by equation (11)
c_p	specific heat at constant pressure [$J kg^{-1} K^{-1}$]
D	hydraulic diameter of unit cell in the combustor [m]
D_c	diameter of the combustor [m]
D_i	effective diffusion coefficient of species i [$m^2 s^{-1}$]
E	activation energy [$J mol^{-1}$]
E^0	incoming radiation from the surroundings [$W m^{-2}$]
E_s	black body total hemispherical emissive power, σT_s^4 [$W m^{-2}$]
f_a	ratio of the cross-sectional area of the solid to that of the gas
f_c	side heat loss factor
h	heat transfer coefficient [$W m^{-2} K^{-1}$]
L	length of the combustor [m]
Le_i	Lewis number of species i
m	mass flow rate of the mixture [$kg m^{-2} s^{-1}$]
Pe	Peclet number defined by equation (11)
Q_{ch}	heat of reaction [$J kg^{-1}$]
Q_r	net radiation from the solid [$W m^{-2}$]
R	universal gas constant, 8.31434 $J mol^{-1} K^{-1}$
r	mass-flow-rate ratio
St	Stanton number defined by equation (11)
T	temperature [K]
T_{af}	adiabatic flame temperature [K]
u	flow velocity of the mixture [$m s^{-1}$]
W_i	molecular weight of species i [$kg mol^{-1}$]
X	space coordinate [m]
X_f	flame position in the combustor [m]
Y_i	mass fraction of species i.

Greek symbols

α	reduced flame temperature defined by equation (11)
β	Zeldovich number defined by equation (11)
Δ	thickness of the reaction zone [m]
ε	emissivity of the solid of the combustor
κ	ratio of conductivities defined by equation (11)
Λ_o	burning velocity eigenvalue of ordinary premixed flame
λ	thermal conductivity [$W m^{-1} K^{-1}$]
ν	stoichiometry, $\nu_f W_f / \nu_o W_o$
ν_i	stoichiometric coefficient of species i
ρ	density of the mixture [$kg m^{-3}$]
σ	Stefan–Boltzmann constant, $5.729 \times 10^{-8} W m^{-2} K^{-4}$
ϕ	equivalence ratio
Ψ	reaction rate [$m^{-3} s^{-1}$].

Subscripts

b, u	burned and unburned gas state, respectively
f, o	fuel and oxidizer
g, s	gas and solid.

stainless steel meshes [9], or of a refractory tube [10]. The mechanisms of heat transfer of these combustors are substantially identical to those of the spongy porous medium. In the tube type combustor, of course, the heat conduction of the solid phase is also an important mechanism of heat transfer while the heat transfer between the gas and solid is small compared to that of the spongy porous medium, and the radiation is described for the tube wall [11]. Among them, the combustor of narrow tubes used by Kotani *et al.* [6] is similar to the present one of the honeycomb ceramic, but the external heat exchangers are coupled with their excess enthalpy burner to burn the ultra-lean mixtures so that the effects of heat recirculation due to the combustor itself are not clearly distinguished from those due to the heat exchangers. The current findings from the existing experiments are the higher flame temperature than the adiabatic flame temperature at that equivalence ratio, a considerable extension of the ranges of flammability and flame stability, and the good emission characteristics of NO_x and CO. These experimental results are qualitatively consistent with the previous theoretical predictions. However, fundamental experimental data on this combustion system such as the thermal structure and flame behaviour in the combustor are not yet available, which is partly due to the difficulties in measurements, particularly in the temperature measurement of the gas phase, caused by the geometrical characteristics of the solid combustor. Furthermore, the flame may be highly two-dimensional in the cross-section of the combustor as seen in this work, while the existing experimental works presumed the one-dimensional flame in the combustor.

This paper presents results of an experimental and theoretical study of the laminar premixed combustion inside a combustor of honeycomb ceramic. The investigation is undertaken in order to obtain the fundamental experimental data and to further the physical understanding of this combustion system. The combustion stability and flame behaviour are tested with variation of the flow rate and equivalence ratio,

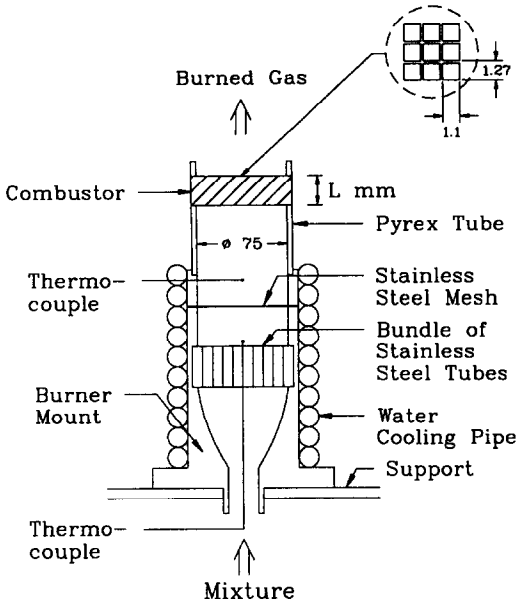

FIG. 1. Schematic of burner system.

and detailed temperature measurements are made separately for the gas and for the solid wall of the combustor. The cross-section of the combustor is also examined by cutting the combustor after burning, in order to confirm the position and distribution of the reaction zone in the combustor. At the same time, a theoretical analysis is conducted to reproduce the experimental results and to clarify the mechanisms of heat transfer involved in this combustion system. Although the analytical model is based on the one-dimensional flame theory, a reasonable quantitative agreement is achieved between the analysis and experiment. A remarkable result of the calculation, also experimentally observed in the case of a highly two-dimensional flame, is the existence of the flame of lower burning velocity and lower flame temperature than for the ordinary premixed flame, which is in conflict with the characteristics of an excess enthalpy flame. It is noted that the present combustor has essentially the same mechanisms of heat transfer as the spongy porous medium, but is of well-defined geometry to facilitate the experimental measurements and the precise analytical description of these mechanisms.

2. EXPERIMENTS

2.1. *Experimental setup and procedure*

The experiment was performed using an experimental burner as shown in Fig. 1. The mixture of propane and air was introduced into the burner. The fuel and the air were continuously supplied by the fuel tank and by the air compressor, respectively. The flow rates were metered separately by the calibrated orifices installed in each feed line. The supplied mixture passed through a bundle of stainless steel tubes of 3 mm in diameter and a stainless steel grid of 100 meshes, and then burned down in a combustor of length L, finally exhausted into the open atmosphere. The bundle of tubes was used to make a uniform flow and the grid to prevent the bundle from heating by the thermal radiation from the combustor. The burner mount was cooled by the water cooling pipe. In order to observe the behaviour of the flame, the pyrex tube of 75 mm i.d. was installed between the combustor and the burner mount. Two chromel–alumel thermocouples of 0.25 mm in diameter were set in front of the combustor to monitor the experiments. A cylindrical honeycomb ceramic combustor of 76 mm in diameter has the nominal cell density of 400 square cells per square inch; a hydraulic diameter of a unit square cell is 1.1 mm and the fraction of the open frontal area is 75% which is equivalent to the porosity. The major phase of the solid is 'cordierite' (magnesium luminosilicate: $2MgO\ 2Al_2O_3\ 5SiO_2$) and its melting point is 1465°C.

Temperature measurements were conducted separately for the gas mixture and for the solid of the combustor. The solid temperature was measured by a 0.1 mm Pt–Pt/13%Rh thermocouple traversed along a centre cell of the combustor and its junction was in contact with the wall of the cell. The gas temperature was also measured by a 25 μm Pt–Pt/13%Rh thermocouple of 20 mm in length perpendicular to the flow direction. In order to prevent the thermocouple from contact with the wall and to traverse it along the combustor, a slit of 26×1.1 mm was made at the centre of the combustor by removing the walls of 20 cells. The thermocouples were supported by the same materials of 0.5 mm in diameter, and their translation was calibrated by a measuring microscope. The recorded temperatures were not corrected for losses.

Two significant parameters in this study are the equivalence ratio, ϕ, and the mass-flow-rate ratio, r. The mass-flow-rate ratio, instead of the volume flow rate, is defined as follows:

$$r = \frac{m_m}{m_o} = \frac{\rho_m u_m}{\rho_o u_o} \tag{1}$$

where m_m is the mass flow rate of the mixture supplied to the combustor and m_o the mass burning velocity of the ordinary premixed flame. It seems desirable to use this ratio rather than the absolute volume flow rate, since the flow rate strongly depends on the size of the combustor [6]. Normal burning velocity of the ordinary premixed flame, u_o, was referred from the experimental data for a propane and air mixture [12]. It is noted here that the mass-flow-rate ratio, r, is based on the flow velocity, u_m, coming into the combustor, so the flow velocity or the mass-flow-rate ratio in a cell of the combustor is 1.33 times above that in equation (1), considering the fraction of the open frontal area.

The experiment was started by supplying the mix-

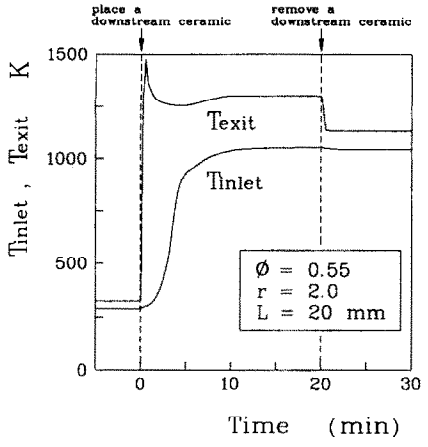

FIG. 2. Starting characteristics of burner system ($\phi = 0.55$, $r = 2.0$; $L = 20$ mm).

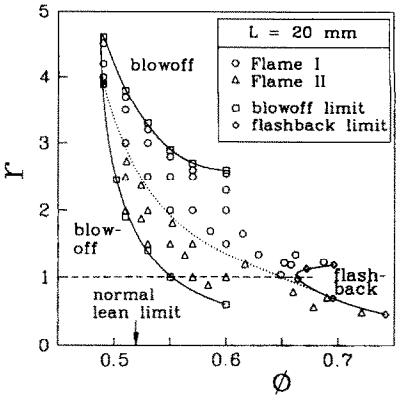

FIG. 3. Stability diagram of the combustor of 20 mm long in the plane of mass-flow-rate ratio (r) and equivalence ratio (ϕ).

ture of relatively small flow rate and high equivalence ratio to produce a stable flame downstream out of the combustor. It was easily made by heating the combustor to put this flame into the combustor; another honeycomb ceramic was placed behind the flame, heated to emit strong thermal radiation which in turn heated the combustor. After the flame completely got into the combustor, the downstream ceramic was removed and the mixture of prescribed equivalence ratio and flow rate was supplied. Figure 2 shows an example of the starting characteristics of the present burner system with the condition of $r = 2.0$ and $\phi = 0.55$. T_{inlet} and T_{exit} are the solid temperatures at the inlet and the exit of the combustor, respectively. After the downstream ceramic was in position, it took the flame about 5 min to enter the combustor completely, and about 20 min to become steady to some extent. The response time was about 5 min to reach the steady state after removing the downstream ceramic.

Various starting procedures had no influence on the final steady state of the flame in the combustor. The steady state was presumed to have been reached when none of the temperatures measured in front of the combustor changed by more than 1°C, and then all the measurements were made. The multiple stationary states of the flame, reported in the combustor of a refractory tube [10], were not found. The reproducibility of experiment was fairly good; for example, variations of the measured temperatures in front of the combustor were less than 5% of their mean values from day to day.

2.2. *Stability characteristics*

Figure 3 shows a stability diagram of the flame in the combustor of 20 mm long in the plane of the equivalence ratio, ϕ, and the mass-flow-rate ratio, r. This diagram was obtained by changing the equivalence ratio and the flow rate from the stable condition. Although heat loss from the combustor might exist in this combustion system, it is possible to make the stable flame in the combustor until the propane–air mixture as lean as equivalence ratio of 0.49 which is lower than the normal lean limit of flammability, $\phi = 0.52$. Two types of stable flame are generally observed which are called flames I and II, divided by a split line (a dotted line in the figure). In the case of flame I, the reaction zone exists in the whole combustor even around the outer wall of the combustor, and for the other case a part of the reaction zone specially at the edge of the combustor emerges from the exit rim of the combustor. Increasing the equivalence ratio and the flow rate, flame II changed to flame I, and vice versa. These flame types to be classified from the distribution of the reaction zone could be distinguished more clearly by their soot lines discussed later.

In this study, the blowoff means that the flame could not be stabilized in the combustor since the flame moves downstream, and the flashback is defined when the flame propagates upstream. The blowoff takes place from flame II as well as from flame I. The blowoff of the flame starts at the exit rim and then extends to the central part of the combustor, which means that the blowoff is affected significantly by the conditions at the combustor wall. It is noted that the blowoff appears rather than the flashback until the equivalence ratio of 0.66, although the flow rate is less than the normal burning velocity. Both the blowoff curves increase exponentially with decreasing equivalence ratio, merging at one point. This point is considered as the lean limit of the present combustor, about $\phi = 0.49$. When the equivalence ratio is above 0.66, on the other hand, the flashback also occurs in both cases of flame I and flame II and the flashback curves take the place of the split line. Flame I is produced for the flow rate between the upper limits of blowoff and flashback, while flame II is between the lower limits although its flow rate is lower than the normal burning velocity. The measured pressure drop

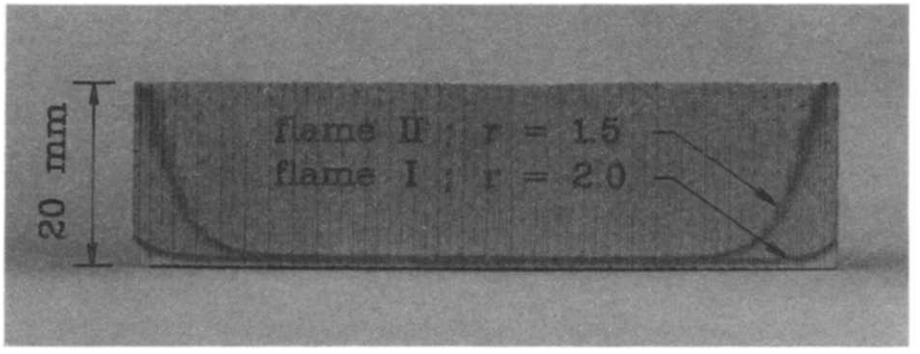

(a)

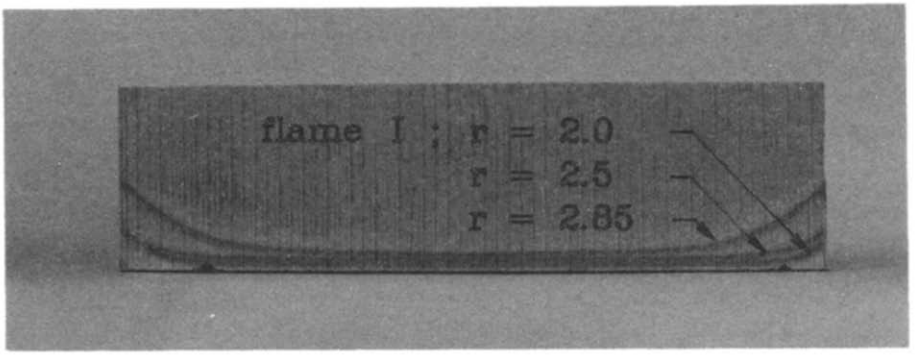

(b)

FIG. 4. Soot lines: (a) flames I and II ($\phi = 0.55$, $L = 20$ mm; $r = 2.0$, 1.5); (b) flame I ($\phi = 0.55$, $L = 20$ mm; $r = 2.0$, 2.5, 2.85).

across the combustor is less than 10 mmH_2O in the range of mass flow rate and equivalence ratio of Fig. 3. Hence, the flame stability and behaviour of the present combustion system are considered to be hardly affected by the pressure effects.

2.3. *Soot lines*

In order to confirm the position of the reaction zone in the combustor, cross-sections of the combustor are examined by cutting the combustor after burning at each flow condition. A dark line is observed in the cross-section of the combustor in which the flame has been made, as shown in Fig. 4. This line might be formed by deposition of soot particles produced by the pyrolysis of the propane in the vicinity of the reaction zone, particularly of the preheat zone. From the soot line, the position and distribution of the reaction zone could readily be confirmed.

Figure 4 shows the soot lines produced in the combustor of 20 mm in length in the flow direction, for various mass-flow-rate ratios and a fixed equivalence ratio of 0.55. From the soot lines of $r = 2.0$ and 1.5 in Fig. 4(a), two types of stable flame mentioned on the previous part could be clearly defined as flames I and II. Flame I is totally inside of the combustor with a nearly one-dimensional shape, while flame II takes a highly two-dimensional shape, part of which gets out of the exit rim and part of which remains one-dimensional in the upstream central region of the combustor. In the very vicinity of the combustor wall, however, flame I also is a little two-dimensional due to the heat loss to the surroundings. An increase of the mass flow rate extends distinctly the two-dimensional region as shown in Fig. 4(b). Considering the two-dimensional distribution, all the measurements of this work were performed in the one-dimensional region. This two-dimensional distribution of the reaction zone is considered due to the heat loss from the outer wall of the combustor, which would exist in the most practical combustors since it is impossible to insulate the com-

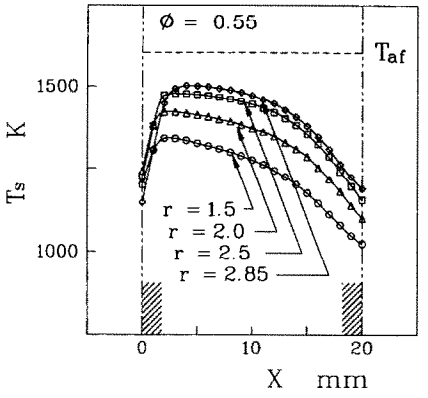

FIG. 5(a). Solid temperature distributions along the flow direction; effects of mass flow rate ($\phi = 0.55$, $L = 20$ mm; $r = 1.5, 2.0, 2.5, 2.85$).

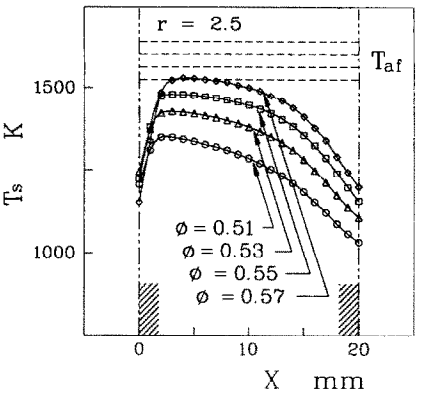

FIG. 5(b). Solid temperature distributions along the flow direction; effects of equivalence ratio ($r = 2.5$, $L = 20$ mm; $\phi = 0.51, 0.53, 0.55, 0.57$).

bustor completely. However, the one-dimensional reaction zone might be maintained in the main central region of the combustor so that the analysis based on the one-dimensional flame theory seems not to be far from reality.

At the mass-flow-rate ratio of 2.0, the location of the flame front is closer to the upstream end of the combustor than at any other ratios of Fig. 4. It can be seen from the stability diagram of Fig. 3 that this mass flow rate is very adjacent to the split line dividing the flame types (dotted line in Fig. 3) when the equivalence ratio is 0.55. Hence, it may be concluded that the mass flow rate just on the split line of the stability diagram produces the flame the most upstream of the combustor when the equivalence ratio is fixed. A similar conclusion may also be made for various equivalence ratios and a fixed r. As observed in the experiment, the flame (flame I) moves upstream in the combustor until the mass flow rate (or the equivalence ratio) decreases to a value on the split line of the stability diagram, but changes abruptly its shape to the highly two-dimensional one (flame II) and then moves downstream conversely as the flow rate decreases more and more, and finally blows off from the combustor. This flame behaviour with the mass flow rate will be discussed later in more detail, and agrees well with the analytical results.

2.4. *Temperature distributions*

The temperature distributions of the solid and the gas separately measured in the combustor of 20 mm long are shown in Figs. 5 and 6. The abscissa is the space coordinate along the flow direction, originated at the inlet of the combustor. These experimental data were mainly obtained at the center region of the combustor, in which the one-dimensional reaction zone might be maintained. The horizontal line T_{af} represents the adiabatic flame temperature calculated for the mixture initially at room temperature of $T_u = 23$°C by using the chemical equilibrium code.

The individual distribution of the solid temperature, measured along the centre cell of the combustor, could be divided into three regions along the combustor as shown in Fig. 5; the upstream region undergoing the rapid increase in the solid temperature, the middle region nearly under the thermal equilibrium state, and finally the downstream region significantly affected by the radiative heat loss to downstream atmosphere. It can be seen from the location of the soot line that the flame exists in the upstream region for most of the incident conditions.

Figure 5(a) shows the effects of the flow rate on the solid temperature distribution. The equivalence ratio is fixed at 0.55. Both the maximum and the exit temperature increase with the flow rate. The mass-flow-rate ratio of 2.0, on the other hand, produces the higher inlet temperature and the narrower upstream region than any other flow rates. That is, the flame is nearest to the upstream end of the combustor when r is about 2.0 in this combustion system. This behaviour agrees with that of the soot lines shown in Fig. 4. The

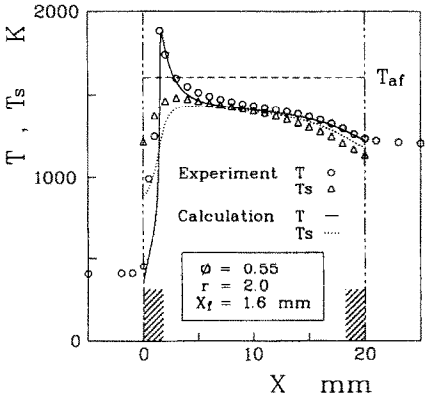

FIG. 6. Temperature distributions measured and computed for a slit. The computed mass-flow-rate ratio in a slit is 4.33 which is about 1.63 times above that in the other cells of the combustor ($\phi = 0.55$, $r = 2.0$; $L = 20$ mm).

effects of the equivalence ratio on the temperature distributions are shown in Fig. 5(b). The mass-flow-rate ratio is fixed at 2.5 so that the absolute flow rate increases with the equivalence ratio. The effects of the equivalence ratio are very similar to those of the flow rate; both the maximum and the exit temperature increase with the equivalence ratio, but the inlet temperature is highest at the equivalence ratio of 0.53 which is more adjacent to the split line of the stability diagram than any other equivalence ratio of Fig. 5(b). The behaviour of the temperature distributions confirms the previous conclusion that the incident condition of the mass-flow-rate ratio and equivalence ratio on the split line of Fig. 3 would make the flame in the most upstream of the combustor.

Figure 6 shows the temperature distributions of the gas mixture and the solid wall of the combustor when $\phi = 0.55$ and $r = 2.0$. This incident condition is in the range of flame I. T and T_s represent the temperatures of the gas and the solid, respectively, which were measured separately along a slit of 26×1.1 mm and along the cell just beside this slit. X_f is the flame position which was measured from the downstream end of the soot line in the slit. In this figure, the computed profiles of temperatures are also shown in reasonable agreement with the experimental values, but will be discussed in the later part of this paper. The solid temperature distribution of Fig. 6, compared with that measured at the same incident condition in the combustor of no slit as shown in Fig. 5(a), presents the higher maximum and exit values but the lower inlet value. It means that the flame front must be slightly moved downstream due to the slit prepared to measure the gas temperature, which was also confirmed by the soot line. The flame shift downstream seems to be caused by an increase of the absolute flow rate due to the larger hydraulic diameter of the slit. Strictly speaking, the temperature distributions measured along a slit would have only a qualitative meaning. Nevertheless the tendency of the temperature distribution of the slit wall is not different from that of the cell wall, so we can believe that the flame of the slit would be identical to that of any other cells, at least in the qualitative aspect.

As expected, the flame front is in the upstream region of the solid temperature distribution. The measured flame temperature is much higher than the adiabatic flame temperature at that equivalence ratio. This temperature overshoot without any other external heating is one of the most remarkable features of the present combustion system, and reveals that the enthalpy of the gas mixture is locally enhanced over the total gas enthalpy initially given at room temperature. In this combustion system, the gas enthalpy enhancement would be made by the internal heat recirculation through the solid of the combustor. Behind the flame front, the gas temperature rapidly decreases below the adiabatic flame temperature, which is considered due to the heat transfer to the solid of relatively low temperature. Thereafter the temperature of the burned gas decreases more slowly and shows the distribution very similar to that of the solid. A rapid decrease in the gas temperature behind the flame front might be another feature of the present combustion system which reduces the residence time of the burned gas in the high temperature region.

3. THEORETICAL ANALYSIS

In addition to an experimental study on the laminar premixed flame stabilized in a combustor of honeycomb ceramic, a theoretical study was also conducted to clarify the mechanisms of heat transfer and the characteristics of flame stabilization and behaviour, and to examine the experimental data. The theoretical analysis, furthermore, is expected to apply in the design of the combustor under optimum conditions.

3.1. *Problem formulation and solution method*

A one-dimensional model is adopted for this analysis although the experiment shows a two-dimensional flame shape in the cross-section of the combustor, considering that the flame remains one-dimensional in its main part. A one-dimensional steady, laminar premixed flame is produced inside the square cells of hydraulic diameter D and length L which constitute the combustor of the same geometrical configuration as used in the experiment.

For simplicity of analysis, most of the assumptions on the ordinary laminar premixed flame are imposed on the present combustion system including the dilute approximation [13]. The working gas is assumed to be nonradiative and to undergo an irreversible one-step, two-reactant overall reaction. The solid of the combustor transfers heat in the flow direction by conduction and radiation. For the radiative transfer, the solid of the combustor is considered as a diffuse, gray body with emission, reflection and absorption of wall radiation. Infinite radial conduction of the solid phase is assumed so that there are no radial distributions of the variables. It is also assumed that there are no heterogeneous chemical reactions on the solid surface, and that all the physical properties are constant.

In the present system, two different phenomena with respective characteristic lengths are coupled; one is related with heat transfer in the whole combustor, the other with heat generation released in the reaction region. These have different characteristic lengths, that is, the combustor length (L) and the thickness of the reaction region (Δ), respectively. The present system, on the other hand, is a two-phase system of the gas and the solid fixed in space. Therefore, the governing equations and the boundary conditions need to be described for the respective phenomena and for the respective phases.

For the whole combustor, the energy conservation equations of the gas and the solid are formulated, respectively, as follows:

$$mc_p\frac{dT}{dX}=\frac{d}{dX}\left(\lambda_g\frac{dT}{dX}\right)+v_f W_f Q_{ch}\Psi+\frac{4}{D}h(T_s-T) \quad (2)$$

$$-f_a\frac{d}{dX}\left(\lambda_s\frac{dT_s}{dX}\right)+\frac{4}{D}Q_r=\frac{4}{D}h(T-T_s)-f_c\frac{4(1+f_a)}{D_c}\varepsilon(E_s-E_u^o) \quad (3)$$

where $m=\rho u$ is the mass flow rate in the cell of the combustor. In the above equations, the term $h(T-T_s)$ represents forced-convection heat transfer between the gas and solid where the heat transfer coefficient h is assumed to be constant for a square duct. The last term of equation (3) represents the radiative heat loss to the surroundings from the side wall of the combustor where f_c is the side heat loss factor. f_c is somewhat adjustable because the solid temperature at the combustor wall is not equal to that in the central part of the combustor due to the two-dimensional effects shown in the experiment. It is noted here that the governing equations and boundary conditions are not for a cell of the combustor, but for the whole combustor of diameter D_c.

Q_r is the net radiative heat flux governed by the radiative transfer equation

$$\frac{d^2Q_r}{dX^2}-\frac{4\varepsilon}{D^2}Q_r=\varepsilon\frac{d^2E_s}{dX^2} \quad (4)$$

where $E_s=\sigma T_s^4$ is the black body total hemispherical emissive power. This transfer equation which is induced from the Fredholm integral equation of the second kind by using a separable kernel approximation is generally good as discussed in the Appendix. It is noted that equation (4) is substantially identical to the transfer equation of a two-flux approximation for the gas radiation which is usually used in the analysis of heat transfer through the porous medium. Hence, the present combustion system of honeycomb ceramic is considered to be equivalent to that of the spongy porous medium, although there may be some subsidiary differences due to the geometrical configuration.

For the reaction region of the characteristic length of Δ, the overall continuity equation and the species conservation equation are described

$$\frac{dm}{dX}=0 \quad (5)$$

$$m\frac{dY_i}{dX}=\frac{d}{dX}\left(\rho D_i\frac{dY_i}{dX}\right)-v_i W_i\Psi, \quad i=\mathrm{f,o}. \quad (6)$$

Equation (5) is a trivial equation, but is useful in convergence for the steady state formulation [14]. In equations (2) and (6), the reaction rate Ψ is expressed in Arrhenius form for an irreversible one-step, two-reactant overall reaction $(C_3H_8+5(O_2+3.76N_2)\rightarrow 4H_2O+3CO_2+18.8N_2)$ with an activation energy of $E=37.2$ kcal mol^{-1} and with an assumption of first order in both fuel and oxygen, proposed by Lavoie [15]

$$\Psi=BY_fY_o\exp\left(-\frac{E}{RT}\right). \quad (7)$$

It is noted that the reaction rate is identically zero outside of the reaction region.

The momentum conservation equation for the one-dimensional deflagration is simply that the pressure is constant. In the combustion system such as the present one, the ideal-gas equation of state may be affected by the pressure loss due to the presence of the combustor although the momentum equation may not, which in turn leads to density variation. From the experiment, it has been found that the pressure drop across the combustor is less than 10 mmH_2O which contributes to about 0.1% of the density variation. Hence the pressure effects are negligible at least in the combustion system of this work.

The space coordinate, X, is originated from the inlet of the combustor. For the combustor of length L, the mixed boundary conditions are given at the inlet and the exit of the combustor, respectively

$$\begin{aligned}
X=0;\quad & -\lambda_g\frac{dT}{dX}+mc_p(T-T_u)=0\\
& -\lambda_s\frac{dT_s}{dX}+\varepsilon(E_s-E_u^o)=0\\
& \frac{dQ_r}{dX}-\frac{2}{D}Q_r=\varepsilon\left\{\frac{dE_s}{dX}-\frac{2}{D}(E_s-E_u^o)\right\}\\
X=L;\quad & \lambda_s\frac{dT_s}{dX}+\varepsilon(E_s-E_b^o)=0\\
& \frac{dQ_r}{dX}+\frac{2}{D}Q_r=\varepsilon\left\{\frac{dE_s}{dX}+\frac{2}{D}(E_s-E_b^o)\right\}.
\end{aligned} \quad (8)$$

When the reaction region of thickness Δ starts at $X=X^*$

$$\begin{aligned}
& X=X^*;\quad \rho D_i\frac{dY_i}{dX}=m(Y_i-Y_{iu}),\quad i=\mathrm{f,o}\\
& X=X^*+\Delta;\quad Y_f=Y_{fl}\rightarrow 0,\\
& \qquad Y_o=Y_{ou}-vY_{fu},\quad \frac{dY_f}{dX}=0
\end{aligned} \quad (9)$$

which are made for the lean mixture ($\phi<1$). Another boundary condition is the overall energy conservation expressed by

$$\begin{aligned}
mc_p(T_{af}-T_u)=\ & mc_p(T_b-T_u)\\
& +(2+\varepsilon f_a)\{E_s(0)+E_s(L)-E_u^o-E_b^o\}\\
& -\frac{2}{\varepsilon}\{Q_r(0)+Q_r(L)\}+f_c\frac{4(1+f_a)}{D_c}\varepsilon\int_0^L(E_s-E_u^o)\,dX
\end{aligned} \quad (10)$$

where subscripts u and b represent far upstream and downstream from the combustor, respectively.

The equations and boundary conditions are then transformed into dimensionless forms. The principal dimensionless variables and parameters are defined as

$$x = \frac{X}{D}, \quad t = \frac{T - T_u}{T_{af} - T_u}, \quad t_s = \frac{T_s - T_u}{T_{af} - T_u},$$

$$q_r = \frac{Q_r}{m_o c_p (T_{af} - T_u)}, \quad y_i = \frac{Y_i - Y_{ib}}{Y_{iu} - Y_{ib}}, \quad r = \frac{m}{m_o(1+f_a)},$$

$$Pe = \frac{m_o c_p D}{\lambda_g}, \quad St = \frac{h}{m_o c_p}, \quad Bo = \frac{4\sigma(T_{af} - T_u)^3}{m_o c_p}$$

$$\kappa = \frac{\lambda_g}{\lambda_s}, \quad f_a = \frac{A_s}{A_g}, \quad Le_i = \frac{\lambda_g}{\rho D_i c_p}, \quad \alpha = \frac{T_{af} - T_u}{T_{af}},$$

$$\beta = \frac{\alpha E}{R T_{af}}, \quad \Lambda_o = \frac{\lambda_g B}{m_o^2 c_p} v_o W_o Y_{fu} \exp\left(-\frac{E}{R T_{af}}\right). \tag{11}$$

The normal mass burning velocity m_o and the adiabatic flame temperature T_{af} are calculated from the experimental data [12] and from the chemical equilibrium code, respectively. The burning velocity eigenvalue Λ_o is taken from the ordinary premixed flame for the same unburned mixture. The geometrical parameters are identical to those in the experiment. For the lean mixture, the properties of the gas are taken for air at a temperature of 1400 K. The properties of the solid are assumed to be the proper values which are in the reliable range for the combustor used in the experiment.

Equations (2)–(10) constitute a system of two coupled boundary-value problems; one is for the whole combustor, the other for the reaction region. The latter undergoes rapid changes in variables to require a number of grid points. The calculation procedure in the present study is to determine the mass flow rate burned down in the reaction region fixed in $(X^*, X^*+\Delta)$. The numerical solution is obtained by employing the finite difference method of PASVA 3, which is suitable to the stiff non-linear boundary-value problem [16]. The thickness of the reaction region, Δ, and the initial distributions are taken from the ordinary premixed flame calculated at that equivalence ratio. The final number of the grid points is about 300 in the whole combustor in which about 200 grid points are concentrated in the reaction region.

3.2. *Flame structure*

Figures 7–9 show the computed results for the parameters and conditions of Table 1. All the calculations of this work have been conducted for the mixture initially at room temperature of $T_u = 23°C$ and for the incoming radiation from the black body at temperature T_u, and thus the outgoing thermal radiation from the combustor acts only as the heat loss on this combustion system. The value of f_c in Table 1, which

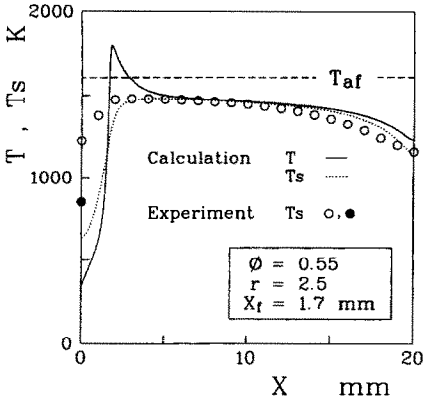

FIG. 7. Computed temperature profiles ($\phi = 0.55$, $r = 2.5$; $L = 20$ mm).

is somewhat adjustable, has been chosen to reproduce properly the experimental results such as the temperature profiles and the flame positions. A detailed survey of the related parameters and conditions is beyond the scope of this work, but their effects should be clarified in further works.

The computed solid temperature profile is compared in Fig. 7 with the experimental values measured by the thermocouple traversed along the centre cell of the combustor. The incident conditions of both the calculation and experiment are identical, $\phi = 0.55$ and $r = 2.5$. For this equivalence ratio, the normal burning velocity of the ordinary premixed flame, u_o, is calculated as 0.104 m s^{-1} from the experimental data [12]. X_f, the flame position, defined as the position of the maximum reaction rate, is 1.7 mm which also agrees with the downstream end of the one-dimensional central part of the soot line within an acceptable measurement error. It is noted here that the mass-flow-rate ratio of 2.5 is a computed value for a given flame position.

Near the inlet of the combustor, the computed solid temperature profile of Fig. 7 is somewhat inconsistent with the experimental values. It may be caused by the effects of property variations which have not been

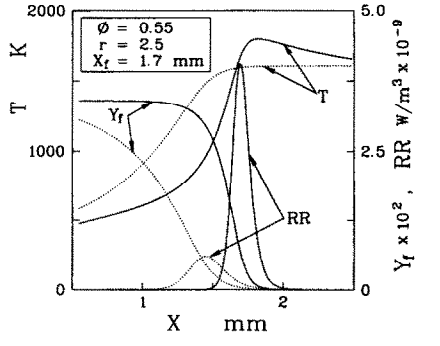

FIG. 8. Magnified flame structure in the reaction region. Dotted lines represent the structure of the ordinary premixed flame ($\phi = 0.55$, $r = 2.5$; $L = 20$ mm).

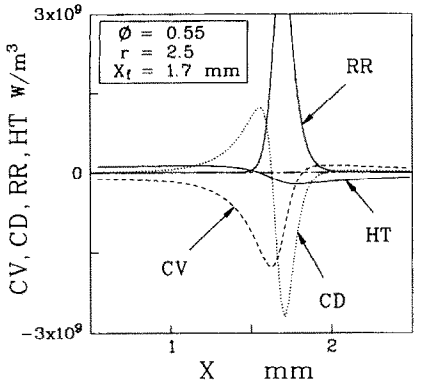

FIG. 9(a). Local energy balance of gas phase in the reaction region. CV, CD, RR and HT are the heat flows into the control volume of gas phase by convection, conduction, chemical heat generation and heat transfer between two phases, respectively ($\phi = 0.55$, $r = 2.5$; $L = 20$ mm).

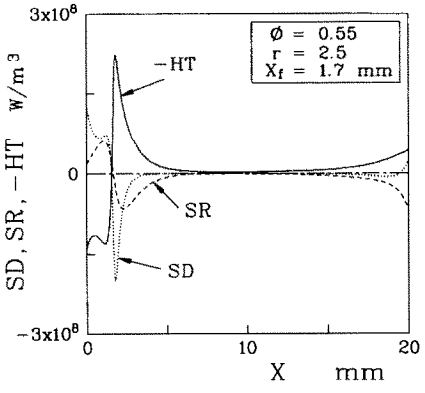

FIG. 9(b). Local energy balance of solid phase in the combustor. SD, SR and $-$HT are the heat flows into the control volume of solid phase by conduction, radiation and heat transfer between two phases, respectively ($\phi = 0.55$, $r = 2.5$; $L = 20$ mm).

Table 1. Parameters and conditions for numerical calculation

ϕ	0.55	Pe	1.825
α	0.815	St	0.874
β	9.518	Bo	3.432
Le_f	1.525	κ	0.162
Le_o	0.832	ε	0.4
Λ_o	41.017	f_c	0.3
f_a	0.333	y_{fi}	10^{-4}
D	1.1 mm	L	20 mm

considered in the analysis, but seems largely due to the problem of temperature measurement. In the upstream region where the temperature rapidly increases, the solid temperature measured along a cell would be higher than the real one by the heat transfer along the thermocouple wires and supports. A solid circle in this figure denotes the solid temperature measured by the thermocouple imbedded at the inlet, which is much lower than that measured along a cell and becomes close to the computed one. Nevertheless, the good agreement between the computed and experimental results is achieved, particularly in the qualitative aspect, considering the gross approximation of the reaction rate and various parameters. The computed profile of gas temperature, on the other hand, is compared with the experimental values measured along a slit as shown in Fig. 6, since the gas temperature could not be measured in a cell of the combustor. The agreement with the experiment is also good, even near the inlet of the combustor. In this case, the calculation was conducted for the parameters different from Table 1, considering the hydraulic diameter of the slit which is about two times as large as that of a cell. The computed mass-flow-rate ratio in a slit is 4.33 which is about 1.63 times above that in the other cells of the combustor, which is consistent with the previous experimental observation that the mass flow rate is increased due to the larger hydraulic diameter of the slit. It is noted that the unburned mixture of Fig. 6 is preheated to about 120°C in the experiment, while the calculation is for the unburned mixture at room temperature. Nevertheless, the calculation seems to reproduce the experimental results reasonably. Considering that the preheating in the experiment is also a result of heat recirculation due to the upstream thermal radiation outgoing from the combustor, there would be no substantial discrepancies between the calculation and the experiment of this work.

The magnified flame structure in the reaction region is shown in Fig. 8. It is compared with the structure of the ordinary premixed flame represented by dotted lines which also have been used as the initial profiles. The flame in the combustor approaches the hot boundary, the gradients become stiff, and the flame thickness, defined here as the distance between the positions of 1% of the maximum reaction rate, is reduced to 53% of that of the ordinary flame although the maximum of the reaction rate becomes much higher. These are the common phenomena to the premixed flame of increased flow rate, and the reverse would be true for the flame of the flow rate less than the normal burning velocity.

The primary mechanism of enthalpy enhancement in the present system is the forced-convection heat transfer between the gas and the solid of the combustor. It balances the convection of the gas in the upstream of the flame front to enhance the enthalpy of the unburned mixture, but is almost negligible in magnitude in the reaction zone where the conduction and convection of the gas balance the chemical heat release, as shown in Fig. 9(a). Here CV, CD, RR and HT represent the heat flows into the control volume of the gas phase by convection, conduction, chemical heat generation and forced-convection heat transfer between the two phases, respectively. These correspond to the respective terms of equation (2)

$$\text{CV corresponds to } -mc_p\frac{dT}{dX}$$

$$\text{CD to } \frac{\mathrm{d}}{\mathrm{d}X}\left(\lambda_g \frac{\mathrm{d}T}{\mathrm{d}X}\right)$$

$$\text{RR to } v_f W_f Q_{ch} \Psi$$

and

$$\text{HT to } \frac{4}{D} h(T_s - T).$$

In this case, the amount of heat recirculation which is the normalized maximum value to integrate the term HT from the inlet is calculated to 0.28. That is, 28% of total heat release is recirculated into the unburned mixture to enhance its enthalpy, which in turn produces the temperature overshoot. In the solid phase, on the other hand, the heat transfer between the gas and solid is balanced by the conduction and radiation of the solid as shown in Fig. 9(b). Here SD, SR and $-$HT are the heat flows by conduction, radiation of the solid and heat transfer between the two phases, respectively, and correspond to the respective terms of equation (3)

$$\text{SD to } f_a \frac{\mathrm{d}}{\mathrm{d}X}\left(\lambda_s \frac{\mathrm{d}T_s}{\mathrm{d}X}\right)$$

$$\text{SR to } -\frac{4}{D} Q_r$$

and

$$-\text{HT to } \frac{4}{D} h(T - T_s).$$

The radiative heat loss term is not presented in this figure since it is negligible compared to the other terms. The conduction and the radiation of the solid are nearly equivalent in magnitude as well as in direction to balance the heat transfer between the gas and solid. Hence, the heat recirculation of the present combustor is executed both by the conduction and the radiation of the solid. This result is somewhat different from that in the spongy porous medium where the energy feedback or heat recirculation is executed primarily by the radiation of the solid [3]. The heat conduction of the solid, however, is not negligible but could be more important to the heat recirculation than the radiation in the combustor made of narrow tube cells such as the present one. The heat transfer between the gas and solid takes place primarily in the upstream region including the reaction zone. Near the downstream end of the combustor the heat loss becomes dominant by the outgoing thermal radiation emitted from the combustor, but the middle region behind the reaction zone is nearly under the thermal equilibrium state. This fact has also been confirmed by the experimental results on the temperature distribution of the solid phase by dividing the three regions as mentioned earlier.

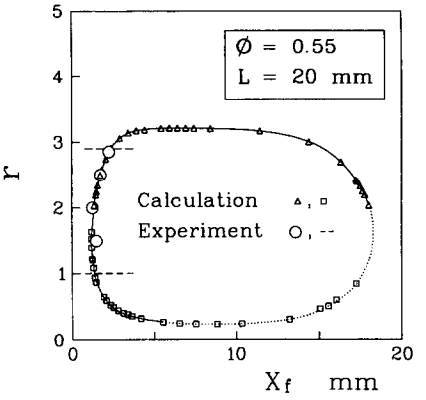

FIG. 10. Relation between mass-flow-rate ratio and flame position. Dashed lines represent the blowoff limits observed in the experiment ($\phi = 0.55$; $L = 20$ mm).

3.3. *Flame behaviours*

Calculations were also performed varying the position of the reaction region in the combustor, but not altering the parameters of Table 1. The computed result is represented by a closed curve in the plane of the mass-flow-rate ratio, r, and the flame position, X_f, as shown in Fig. 10. On the curve, small triangles and squares denote the computed values corresponding to the upper and lower solutions, respectively. The experimental values are also presented by the circles in this figure, which are taken from the soot lines shown in Fig. 4. From the curve, it can be seen that the flame is stabilized downstream as well as upstream of the combustor for an identical flow rate, while the upper and lower solutions of different mass flow rates exist for an identical flame position. The downstream lower solution depicted by a dotted line in this figure is obtained when the fuel mass fraction at the hot boundary of reaction region, y_{fh}, is much more than that of Table 1, which is beyond the scope of this analysis since it means that the hot boundary of the reaction region, namely, the downstream end of the flame is placed outside the combustor.

In the upstream region of the combustor, the computed result agrees reasonably with the experimental values. Some differences between the experimental and computed values would be attributed to the gross approximation of the related physical parameters and to the preheating and two-dimensional effects in the experiment. The upstream upper and lower solutions in the curve would correspond to flames I and II of the experiment, respectively. As observed in the experiment, there exists a mass flow rate which produces the flame at a minimum distance from the upstream end of the combustor. The flame moves downstream as the mass flow rate becomes lower as well as higher than this critical value. The minimum distance is consistent with the position at which the amount of heat recirculation is also minimum. In the upstream region of the combustor, the amount of heat recirculation increases as the flame moves downstream. In the upper solution, the flame shift

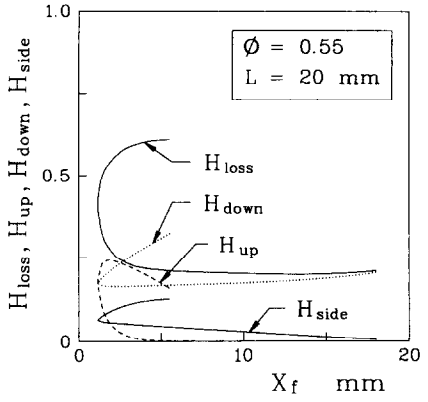

FIG. 11. Overall energy balance with variation of flame position. H_{loss} is the normalized total heat loss from the combustor. H_{up}, H_{down} and H_{side} are the normalized radiative heat losses from the upstream end, the downstream end and the side wall of the combustor, respectively ($\phi = 0.55$; $L = 20$ mm).

downstream seems to be a matter of course, because the convection of the gas increased by the higher mass flow rate requires more heat to be recirculated to the unburned mixture. In the case of the lower solution, it may be explained as follows; when the mass flow rate becomes below the critical value, the heat release from the flame decreases while the heat loss from the combustor relatively increases since it primarily depends on the solid temperature, which is also confirmed by the overall energy balance shown in Fig. 11. In order to overcome the increased heat loss and to sustain the combustion, more heat should be recirculated to the unburned mixture, consequently the flame moves downstream. The other previous works [4, 5] show that there is no minimum distance in the absence of heat loss from the combustor.

The computed mass flow rate has maximum and minimum values, which physically correspond to the upper and lower blowoff limits, respectively. The experimental values are denoted by the dashed lines in this figure. The disparity between the computed and experimental values seems due to the two-dimensional effects, because the blowoff in the experiment starts from the outer wall of the combustor significantly affected by the side heat loss. However, the upper blowoff limit is basically due to the finiteness of the combustor although the other effects such as the heat loss may influence its value, considering that the semi-infinite combustor of Takeno and Sato [1] has no blowoff limits as long as the mixture of increased flow rate is burned down in the reaction zone. When the flame moves downstream from the position of the maximum mass flow rate, the region heated by the burned gas is reduced so that the mean temperature of the solid combustor falls. Consequently the heat recirculated to the unburned mixture is decreased on the whole, which reduces the mass flow rate. The lower blowoff limit, rather than the extinction, is considered due to the heat loss from the combustor in that the adiabatic combustor has no minimum mass flow rate [4]. It is noted that the minimum flow rate is small enough to produce the stable flame of the flow rate less than the normal burning velocity. On the other hand, the stable flame is predicted in the downstream region of the combustor, but not observed in the experiment. The failure in our experiment is thought to be due to the two-dimensional effects in the combustor as aforementioned; the present combustor is composed of numerous cells which are affected by the radial heat loss different from each other. Due to the radial distribution of heat loss, the flame takes a two-dimensional shape in the combustor as seen from the soot line of Fig. 4. The two-dimensional flame becomes so unstable in the downstream region of the combustor that it either moves to the upstream region or blows off from the exit of the combustor. This presumption seems to be plausible from the previous experimental finding of Bernstein and Churchill [10], in which the stationary one-dimensional flame is produced in the downstream as well as in the upstream region of a refractory tube used as a combustor.

Figure 11 shows the results of the overall energy balance with variation of the flame position. H_{up}, H_{down} and H_{side} are the normalized radiative heat loss to the surroundings from the combustor inlet, exit and side wall, respectively. H_{loss} is the total heat loss from the combustor normalized by the total heat release, and hence

$$H_{loss} = H_{up} + H_{down} + H_{side} = 1 - t_b \qquad (12)$$

where t_b is the non-dimensional temperature of burned gas outside the combustor, which means the normalized exit sensible enthalpy flow. Values of H are formulated from equation (10), and presented in this figure for the upper and upstream lower solutions depicted by the solid curve in Fig. 10. In the upper solution, total heat loss undergoes no appreciable changes except near the upstream end of the combustor where the upstream radiative heat loss abruptly increases. When the flame is at the minimum distance, 17% of the total heat release can be converted to the upstream thermal radiation. In the lower solution, on the other hand, total heat loss increases with the flame position, which is consistent with the previous discussion. It is noted here that the heat loss is relative to the mass flow rate and its absolute value decreases with the flame position in the case of the lower solution.

Temperature profiles of the upper and lower solutions are shown in Figs. 12(a) and (b), respectively. The numerals denote the mass-flow-rate ratios corresponding to the profiles. In the case of the upper solution, all the flame temperatures are higher than the adiabatic flame temperature. The maximum flame temperature is obtained at the position of the maximum flow rate which is located slightly upstream rather than at the centre of the combustor. It is seen that the flame behaviour and temperature profiles of the upper solution are in good agreement with those

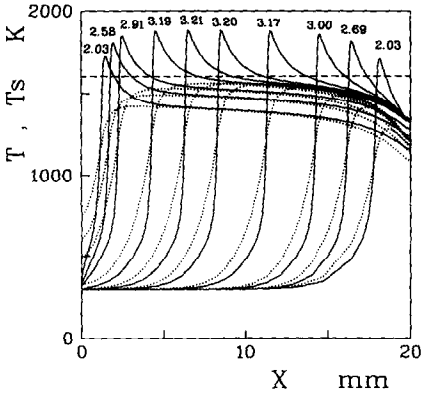

FIG. 12(a). Computed temperature profiles for the upper solution. Numerals denote the mass-flow-rate ratios corresponding to the profiles ($\phi = 0.55$; $L = 20$ mm).

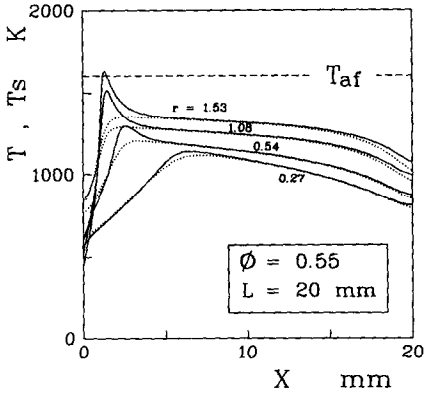

FIG. 12(b). Computed temperature profiles for the lower solution ($\phi = 0.55$; $L = 20$ mm).

of flame I observed in the experiment. On the other hand, the lower solution would correspond to flame II of the experiment. The flame behaviour of the lower solution is also consistent with the observed one, although the abrupt transition to the highly two-dimensional flame could not be predicted by the present analysis. It is noted from the temperature profiles of the lower solution shown in Fig. 12(b) that the flame temperature might be lower than the adiabatic flame temperature for the flow rate less than the normal burning velocity. In this case, the flame is thicker than the ordinary premixed flame, and moreover, the mechanisms of heat transfer in the gas phase are conspicuously different from those of the upper solution. The heat transfer between the gas and solid is not negligible in the enlarged reaction region, but almost equivalent in magnitude to the other mechanisms such as the conduction and convection of the gas phase. The flame characteristics of the lower solution are clearly distinguished from those of the excess enthalpy flame of Takeno and Hase [5] as well as from those of the upper solution, and preferably similar to those of the non-adiabatic flame with heat loss [13]. The lower solution would be another feature of the present combustion system, which contributes to extending the range of the combustion stability for decreased mass flow rates.

4. CONCLUDING REMARKS

This paper has presented some results of an experimental and theoretical study of laminar premixed combustion inside a honeycomb ceramic. The ranges of flammability and flame stability are considerably extended only by the internal heat recirculation, not by any other external heating. Two types of stable flame are observed in the experiment; one is a nearly one-dimensional flame wholly inside the combustor, the other is a highly two-dimensional flame which remains one-dimensional in the central region of the combustor. These correspond to the upper and lower solutions of the analysis based on the one-dimensional flame theory, although the abrupt change of the flame shape is not properly explained by the analysis. The soot line observed in the cross-section of the combustor clearly distinguishes the flame types, and also confirms the position and distribution of the reaction zone.

A line, dividing the flame types in the stability diagram of the present combustion system, provides the incident condition to produce the flame in the most upstream of the combustor. The analysis reveals that this condition requires the minimum heat recirculation to sustain the combustion. The other conditions away from this line move the flame downstream until the corresponding blowoff limits. It is noted that blowoff, not flashback, occurs at the flow rate less than the normal burning velocity, which is considered due to the heat loss from the combustor. Temperature measurements show that the gas temperature would be higher than the adiabatic flame temperature but rapidly decrease behind the flame front, which is attributed to the heat transfer to the solid. The solid of the combustor recirculates the heat released from the reaction zone to the unburned mixture, and also effectively converts it into the outgoing thermal radiation.

The analysis makes a good reproduction of the experimental temperature profiles and flame behaviours, and reveals that the heat recirculation is built up both by the conduction and the radiation of the solid phase. A remarkable result of the calculation, also observed experimentally in the case of the highly two-dimensional flame, is the existence of the flame which has a burning velocity and flame temperature lower than those of the ordinary premixed flame. The characteristics of this flame are inconsistent with those of the excess enthalpy flame, but lead to an enhancement of the flame stability for decreased flow rate. On the other hand, the stable flame is predicted in the downstream region of the combustor, but not observed in the experiment probably because the flame becomes unstable due to the two-dimensional effects of heat loss.

REFERENCES

1. T. Takeno and K. Sato, An excess enthalpy flame theory, *Combust. Sci. Technol.* **20**, 73–84 (1979).
2. F. J. Weinberg, Combustion temperature: the future?, *Nature* **233**, 239–241 (1971).
3. Y. Yoshizawa, K. Sasaki and R. Echigo, Analytical study on the structure of radiation controlled flame, *Int. J. Heat Mass Transfer* **31**, 311–319 (1988).
4. T. Takeno, K. Sato and K. Hase, A theoretical study on an excess enthalpy flame, *Eighteenth Symp. (Int.) on Combustion*, pp. 465–472. The Combustion Institute (1981).
5. T. Takeno and K. Hase, Effects of solid length and heat loss on an excess enthalpy flame, *Combust. Sci. Technol.* **31**, 207–215 (1983).
6. Y. Kotani, H. F. Behbahani and T. Takeno, An excess enthalpy flame combustor for extended flow ranges, *Twentieth Symp. (Int.) on Combustion*, pp. 2025–2033. The Combustion Institute (1984).
7. R. Echigo, Effective energy conversion method between gas enthalpy and thermal radiation and application to industrial furnaces, *Proc. 7th Int. Heat Transfer Conf.*, Munich, Vol. 6, pp. 361–366 (1982).
8. K. Y. Wang and C. L. Tien, Thermal insulation in flow systems: combined radiation and convection through a porous segment, *ASME J. Heat Transfer* **106**(2), 453–459 (1984).
9. R. Echigo, Y. Yoshizawa, K. Hanamura and T. Tomimura, Analytical and experimental studies on radiative propagation in porous media with internal heat generation, *Proc. 8th Int. Heat Mass Transfer Conf.*, San Francisco, Vol. II, pp. 827–832 (1986).
10. M. H. Bernstein and S. W. Churchill, Multiple stationary states and NO_x production for turbulent flames in refractory tubes, *Sixteenth Symp. (Int.) on Combustion*, pp. 1737–1745. The Combustion Institute (1977).
11. B. Choi and S. W. Churchill, A model for combustion of gaseous and liquid fuels in a refractory tube, *Seventeenth Symp. (Int.) on Combustion*, pp. 917–925. The Combustion Institute (1979).
12. Y. Yamaoka and H. Tsuji, Determination of burning velocity using counterflow flames, *Twentieth Symp. (Int.) on Combustion*, pp. 1883–1892. The Combustion Institute (1984).
13. F. A. Williams, *Combustion Theory* (2nd Edn), Chap. 5. Benjamin/Cummings, Menlo Park, California (1985).
14. M. D. Smooke, J. A. Miller and R. J. Kee, Determination of adiabatic flame speeds by boundary value methods, *Combust. Sci. Technol.* **34**, 79–90 (1983).
15. G. A. Lavoie, Correlation of combustion data for S.I. engine calculations—laminar flame speed, quench distance and global reaction rates, SAE Paper 780229, pp. 1015–1033 (1978).
16. V. Pereyra, PASVA 3: an adaptive finite difference FORTRAN program for first order nonlinear ordinary boundary problems, *Lect. Notes Comp. Sci.* **76**, 67–88 (1978).
17. R. Siegel and J. R. Howell, *Thermal Radiation Heat Transfer* (2nd Edn), Chap. 8. McGraw-Hill, New York (1981).
18. J. R. Howell, *A Catalog of Radiation Configuration Factors*. McGraw-Hill, New York (1982).

APPENDIX: RADIATIVE TRANSFER EQUATION

For a square cell of hydraulic diameter D and length L, the radiative heat transfer is governed by the wall to wall radiation. Assuming that the solid of the cell is a diffuse, gray opaque body with emission, reflection and absorption of wall radiation and that the emissivity of the solid is constant, the radiative transfer equation is exactly formulated as follows [17]:

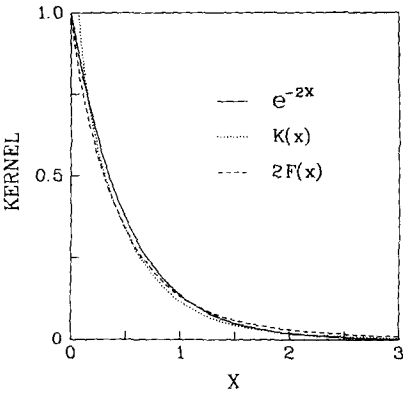

FIG. A1. Configuration factor kernels.

$$Q_r^o-(1-\varepsilon)\int_0^l Q_r^o(\tilde{x})K(|x-\tilde{x}|)\,d\tilde{x}=\varepsilon E_s + (1-\varepsilon)\{E_u^o F(x)+E_b^o F(l-x)\} \quad (A1)$$

where $x = X/D$, $l = L/D$ and the outgoing radiative flux (radiosity), Q_r^o, is

$$Q_r^o = E_s - \frac{1-\varepsilon}{\varepsilon}Q_r. \quad (A2)$$

For the square cross-section of the cell, the configuration factor kernels K and F are [18]

$$K(x)=\frac{1}{\pi}\left\{\frac{\tan^{-1}[(x^2+1)^{-1/2}]}{(x^2+1)^{3/2}}+\tfrac{1}{2}\ln\frac{(x^2+1)^2}{x^2(x^2+2)}\right\} \quad (A3)$$

$$F(x)=\frac{1}{\pi}\left\{\frac{x}{2}\ln\frac{x^2(x^2+2)}{(x^2+1)^2}-\frac{x}{(x^2+1)^{1/2}}\tan^{-1}\frac{1}{(x^2+1)^{1/2}} + \tan^{-1}\frac{1}{x}\right\}. \quad (A4)$$

Equation (A1) is a Fredholm integral equation of the second kind, and yields a system of integro-differential equations with the other differential equations for the present combustion system. To avoid solving the integro-differential equations, equation (A1) should be changed to a differential equation, which can be achieved by the separable kernel approximation [17]. As shown in Fig. A1, the kernels of equations (A3) and (A4) are reasonably approximated by the separable exponential function

$$K(x) \approx \exp(-2x) \quad (A5)$$

$$F(x) \approx \tfrac{1}{2}\exp(-2x). \quad (A6)$$

When the approximate kernels are substituted into equation (A1)

$$Q_r^o-(1-\varepsilon)\left\{\exp(-2x)\int_0^x Q_r^o(\tilde{x})\exp(2\tilde{x})\,d\tilde{x} + \exp(2x)\int_x^l Q_r^o(\tilde{x})\exp(-2\tilde{x})\,d\tilde{x}\right\} = \varepsilon E_s+\frac{1-\varepsilon}{2}\{E_u^o\exp(-2x)+E_b^o\exp[-2(l-x)]\}. \quad (A7)$$

By differentiating the above equation two times, the integrals can be removed and the following differential equation obtained:

$$\frac{d^2Q_r^o}{dX^2}-4\varepsilon Q_r^o=\varepsilon\frac{d^2E_s}{dx^2}-4\varepsilon E_s. \quad (A8)$$

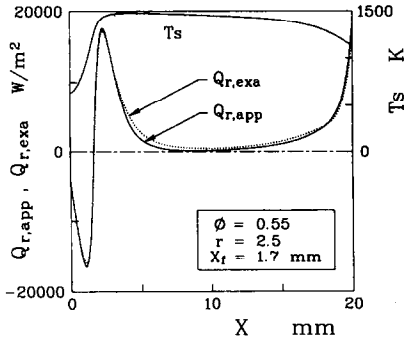

FIG. A2. Net radiative heat fluxes; $Q_{r,exa}$ is for exact kernels, and $Q_{r,app}$ for exponential approximate kernels ($\phi = 0.55$, $r = 2.5$; $L = 20$ mm).

In terms of the net radiative heat flux, Q_r, and the dimensional distance X

$$\frac{d^2Q_r}{dx^2} - \frac{4\varepsilon}{D^2}Q_r = \varepsilon\frac{d^2E_s}{dX^2}. \quad \text{(A9)}$$

Two boundary conditions needed to solve equation (A9) are also obtained by differentiating equation (A7) at $X = 0$ and L

$$X = 0; \quad \frac{dQ_r}{dX} - \frac{2}{D}Q_r = \varepsilon\left(\frac{dE_s}{dX} - \frac{2}{D}E_s + \frac{2}{D}E_u^\circ\right) \quad \text{(A10)}$$

$$X = L; \quad \frac{dQ_r}{dX} + \frac{2}{D}Q_r = \varepsilon\left(\frac{dE_s}{dX} + \frac{2}{D}E_s - \frac{2}{D}E_b^\circ\right). \quad \text{(A11)}$$

To examine the accuracy of this approximation, the net radiative heat fluxes $Q_{r,exa}$ and $Q_{r,app}$ are compared in Fig. A2. $Q_{r,exa}$ is calculated from equation (A1) with the exact kernels of equations (A3) and (A4), while $Q_{r,app}$ from equation (A9) with the boundary conditions of equations (A10) and (A11). These are obtained for an identical solid temperature profile of Fig. 7. A relative error seems to be somewhat large in the region under nearly thermal equilibrium of mild temperature profile rather than near the entrance of the cell where the temperature profile is steep, but its value is small enough to neglect the effects on the heat transfer through the whole combustor. With respect to the outgoing radiative flux, moreover, the maximum difference between them is less than 2%. Hence the separable kernel approximation of this work is thought to be good with an acceptable accuracy, at least without missing the substantial characteristics of radiative heat transfer.

It is instructive to compare this approximation with the two-flux approximation for the gas radiation, usually used in the analysis of heat transfer of the porous system. The transfer equation and boundary conditions of the two-flux gray radiation model are expressed as [8]

$$\frac{d^2\tilde{Q}_r}{dX^2} - 4\sigma_a(\sigma_a + 2b\sigma_s)\tilde{Q}_r = 4\sigma_a\frac{dE_s}{dX} \quad \text{(A12)}$$

$$X = 0; \quad \frac{d\tilde{Q}_r}{dX} - 2\sigma_a\tilde{Q}_r = 4\sigma_a(E_s - E_u^\circ) \quad \text{(A13)}$$

$$X = L; \quad \frac{d\tilde{Q}_r}{dX} + 2\sigma_a\tilde{Q}_r = 4\sigma_a(E_s - E_b^\circ) \quad \text{(A14)}$$

where σ_a, σ_s and b are the absorption coefficient, scattering coefficient and back-scattered fraction factor, respectively, and $\tilde{Q}_r$ is the diffusive radiant heat flux. This two-flux approximation is found to be generally good compared to the exact integral transfer equation for the porous medium in the limiting case of no scattering [8]. Equations (A12)–(A14) become exactly identical to equations (A9)–(A11), respectively, by the following transformation:

$$\frac{d\tilde{Q}_r}{dX} = \frac{4}{D}Q_r, \quad \sigma_a = \frac{\varepsilon}{D} \quad \text{and} \quad 2b\sigma_s = \frac{1-\varepsilon}{D} \quad \text{(A15)}$$

which seems to be compatible with the related physics. By equation (A15), the equivalent absorption coefficient of the present combustor of Table 1 is about 360 m^{-1}, and the optical thickness $(\sigma_a + \sigma_s)L = L/D = 18.2$ when b is assumed to be 0.5. Hence, the present combustion system has essentially the same mechanisms of heat transfer as the porous medium, and moreover may be optically thick in view of the gas radiation compared to the porous medium of Yoshizawa *et al.* [3].

FLAMME LAMINAIRE EN PREMELANGE STABILISEE DANS UNE CERAMIQUE EN NID D'ABEILLE

Résumé—Une flamme laminaire prémélangée dans une céramique en nid d'abeille est étudiée expérimentalement et théoriquement pour fournir des données détaillées pour des approches numériques et pour comprendre mieux les mécanismes de transfert thermique et en particulier la recirculation thermique interne. Les domaines d'inflammation et de stabilité sont sensiblement élargis sans aucun chauffage externe. On observe deux types de flamme stable: l'un est presque monodimensionnel dans le combusteur et l'autre fortement bidimensionnel. Ceci est clairement visible par les lignes de suie dans la section droite du combusteur et ça correspond aux solutions supérieure et inférieure de l'analyse théorique. Des mesures de température montrent une température de gaz supérieure à la température adiabatique de flamme, ce qui est attribuable à une recirculation interne de chaleur. L'analyse basée sur une théorie monodimensionnelle de flamme reproduit raisonnablement les profils de température expérimentaux et les comportements de la flamme, et elle révèle que la chaleur est recirculée au mélange imbrûlé à la fois par conduction et par rayonnement de la phase solide. La flamme stable est aussi prédite dans la région en aval du combusteur, mais elle n'est pas observée dans l'expérimentation, probablement à cause des effets bidimensionnels de perte thermique. Un résultat important de ce travail est l'existence de la flamme à faible vitesse et à basse température, ce qui est différent de l'excès d'enthalpie de la flamme.

STABILISIERUNG EINER LAMINAR VORGEMISCHTEN FLAMME IN EINER WABENFÖRMIGEN KERAMIKSTRUKTUR

Zusammenfassung—Um detaillierte Werte für Berechnungsansätze zu erhalten und das Verständnis der Wärmeübertragungsmechanismen—speziell der internen Rückzirkulation von Wärme—zu verbessern, wurde eine laminar vorgemischte Flamme in einer wabenförmigen keramischen Struktur theoretisch und experimentell untersucht. Die Bereiche der Flammenfront und Flammenstabilität werden ohne äußere Wärmezufuhr beträchtlich erweitert. Es werden zwei Arten von stabilen Flammen beobachtet: die eine ist im Brenner annähernd eindimensional, die andere im hohen Grade zweidimensional. Die beiden Flammenarten können auch eindeutig durch die Rußlinienspuren, die im Brennerquerschnitt beobachtet werden, unterschieden werden. Sie korrespondieren mit den größten und kleinsten Lösungen der theoretischen Berechnungen. Temperaturmessungen zeigen eine höhere Gastemperatur im Vergleich zur adiabaten Flammentemperatur. Dies wird auf eine interne Rückzirkulation von Wärme zurückgeführt. Die Berechnung, die auf der eindimensionalen Flammentheorie beruht, ergibt in etwa die Werte, die dem experimentell ermittelten Temperaturprofil und Flammenverhalten entsprechen. Sie zeigt außerdem, daß Wärme zur nichtverbrannten Brennstoffmischung hin zurückzirkuliert wird. Dieser Transport geschieht sowohl durch Leitung als auch durch Strahlung. Auch für die stromabwärts gelegenen Zonen des Brenners wurde eine stabile Flamme berechnet, die jedoch im Experiment nicht beobachtet wurde, was wahrscheinlich auf die zweidimensionalen Effekte der Wärmeverluste zurückzuführen ist. Ein bemerkenswertes Ergebnis dieser Arbeit ist die Existenz einer Flamme mit niedriger Brenngeschwindigkeit und niedriger Temperatur, die sich von einer Flamme mit Enthalpieüberschuß unterscheidet.

ЛАМИНАРНОЕ ПЛАМЯ ГОРЮЧЕЙ СМЕСИ, СТАБИЛИЗИРОВАННОЕ ВНУТРИ ЯЧЕИСТОЙ КЕРАМИКИ

Аннотация—Экспериментально и теоретически исследуется ламинарное пламя внутри ячеистой керамики с целью получения подробных данных для расчетов и более глубокого физического понимания механизмов теплопереноса, в частности, внутренней рециркуляции тепла. Без применения внешнего нагрева существенно расширены диапазоны воспламеняемости и устойчивости пламени. Наблюдаются два вида устойчивости пламени: один является почти одномерным в камере сгорания, второй—существенно двумерным. Эти виды четко различаются по следам копоти, наблюдаемым в поперечном сечении камеры сгорания, и соответствуют верхнему и нижнему решениям теоретического анализа. Измерения показывают, что температура газа превышает адиабатическую температуру пламени, что объясняется внутренней рециркуляцией тепла. Анализ на основе теории одномерного пламени удовлетворительно воспрроизводит экспериментальные температурные профили и поведение пламени и показывает, что тепло передается к негорящей смеси за счет теплопроводности и излучения твердой фазы. Теория предсказывает также существование устойчивого пламени в области вниз по течению, однако экспериментально оно не наблюдается, по-видимому, из-за двумерных эффектов тепловых потерь. Существенным результатом работы является обнаружение пламени с низкими скоростью горения и температурой, в отличие от пламени с избыточной энтальпией.